crystals

MDPI

Article

In Vitro Physical Characterizations and Docking Studies on Carvedilol Nanocrystals

Jamal Moideen Muthu Mohamed [1], Ali Alqahtani [2], Farid Menaa [3,*], Saminathan Kayarohanam [4], Adel Al Fatease [5], Taha Alqahtani [2], Ali Alamri [5], Mohamed El-Sherbiny [6], Sundarapandian Ramkanth [7] and Ashok Kumar Janakiraman [8,*]

1 Vaasudhara College of Pharmacy, Sante Circle, Hoskote 562114, Karnataka, India; jmuthumohamed@gmail.com
2 Department of Pharmacology, College of Pharmacy, King Khalid University, Guraiger, Abha 62529, Saudi Arabia; amsfr@kku.edu.sa (A.A.); ttaha@kku.edu.sa (T.A.)
3 Department of Nanomedicine, California Innovations Corporation, San Diego, CA 92037, USA
4 Faculty of Bio-Economy and Health Sciences, Geomatika University College, Kuala Lumpur 54200, Malaysia; saminathan@geomatika.edu.my
5 Department of Pharmaceutics, College of Pharmacy, King Khalid University, Guraiger, Abha 62529, Saudi Arabia; afatease@kku.edu.sa (A.A.F.); aamri@kku.edu.sa (A.A.)
6 Department of Basic Medical Sciences, College of Medicine, AlMaarefa University, Riyadh 11597, Saudi Arabia; msharbini@mcst.edu.sa
7 Department of Pharmaceutics, Karpagam College of Pharmacy, Coimbatore 641032, Tamil Nadu, India; ramkanth@kcp.edu.in
8 Faculty of Pharmaceutical Sciences, UCSI University, Cheras, Kuala Lumpur 56000, Malaysia
* Correspondence: menaateam@gmail.com (F.M.); ashok@ucsiuniversity.edu.my (A.K.J.)

check for updates

Citation: Mohamed, J.M.M.; Alqahtani, A.; Menaa, F.; Kayarohanam, S.; Fatease, A.A.; Alqahtani, T.; Alamri, A.; El-Sherbiny, M.; Ramkanth, S.; Janakiraman, A.K. In Vitro Physical Characterizations and Docking Studies on Carvedilol Nanocrystals. *Crystals* **2022**, *12*, 988. https://doi.org/10.3390/cryst12070988

Academic Editors: Łukasz Szeleszczuk, Dariusz Maciej Pisklak, Monika Zielińska-Pisklak and Borislav Angelov

Received: 8 June 2022
Accepted: 12 July 2022
Published: 16 July 2022

Publisher's Note: MDPI stays neutral with regard to jurisdictional claims in published maps and institutional affiliations.

Copyright: © 2022 by the authors. Licensee MDPI, Basel, Switzerland. This article is an open access article distributed under the terms and conditions of the Creative Commons Attribution (CC BY) license (https://creativecommons.org/licenses/by/4.0/).

Abstract: The major goal of this investigation was to prepare carvedilol nanocrystals (CRL-NCs) for better solubility, stability, and bioavailability. Using polyvinyl pyrolidine K-30 (PVP) and sodium dodecyl sulphate (SDS) as stabilisers, CRL-NCs were effectively synthesised by emulsion-diffusion, followed by the high-pressure homogenization (HPH) method. The A_L classes of phase solubility curves with ideal complexes produced with stabilisers were estimated by thermodynamic parameters. The docking study was performed with the active site of a β-1 adrenoreceptor protein, and the CRLs docking score was revealed as -23.481 Kcal/mol^{-1}. At 25 and 37 °C, the optimum interaction constant was determined for PVP (144 and 176 M^{-1}) and SDS (102 and 121 M^{-1}). The average particle size (PS) of the produced stable CRL-NCs is 58 nm, with a zeta potential of -27.2 ± 2.29 mV, a poly dispersibility index of 0.181 ± 0.012, a percentage yield of 78.7 ± 3.41, drug content of 96.81 ± 3.64%, and entrapment efficiency of 83.61 ± 1.80%. The morphological data also reveals that the CRL-NCs were nearly sphere shaped, with distinct and smooth surfaces. CRL-NCs were studied using X-ray diffraction (XRD), fourier transform infrared (FT-IR) spectroscopy, and differential scanning calorimetry (DSC), and the results show no chemical structural alterations, even when PS was reduced. NCs accelerate their in vitro dissolution release rate by about three times faster than CRL-MCs (microcrystals). When kept at 4 °C, the CRL-NCs exhibit good physical stability for six months. As a result, the CRL-NCs created via emulsion-diffusion followed by HPH with stabilisers can be used to increase the solubility, stability, and bioavailability of poorly soluble or lipophilic drugs.

Keywords: nanocrystals; emulsion-diffusion method; docking study; phase solubility study; carvedilol; polyvinyl pyrolidine K-30

1. Introduction

An increasing number of poorly soluble or lipophilic drugs necessitates a novel strategy for achieving the appropriate bioavailability after delivery. Many methods were established to enhance the solubility and improve the dissolution of poorly water-soluble drugs, including salt formation, solid dispersion, inclusion complex, micronization, and

others [1], all of which aim to increase the wettability, solubility, and surface area of drug particles. The thermal and chemical deterioration of the product owing to high temperature, high energy needs, greater solvent consumption, solvent residues, and a broad particle size (PS) range are the main limitations of these traditional processes [2]. As seen by the small number of medications available on the market, these formulation techniques achieve little success.

Carvedilol (CRL) is a β-adrenergic (nonselective) blocking agent with α1-blocking activity that is extensively prescribed in the treatment of essential hypertension, angina pectoris, and congestive heart failure. CRL, a poorly water soluble (0.583 $mg \cdot L^{-1}$) and highly permeable drug, belongs to the BCS class-II category. Poor water solubility means that absorption is restricted by dissolving rate, resulting in insufficient and delayed absorption [3]. Developing an appropriate method to improve in vitro dissolution for drug products with limited water solubility is a challenge for scientists.

In recent years, several novel medications successfully reduced their solubility to the point that micronization was no longer adequate to provide excellent bioavailability. As a result, the next stage was to attain nano size; nanonisation is one such method for increasing drug solubility. Nanosuspension not only solves the problem of low solubility and bioavailability, but it also alters the pharmacokinetics of the drug, enhancing the safety and efficacy [4]. Pharmaceutical nanosuspensions are described as highly fine colloid, biphasic, and dispersed solid drug particles in an aqueous media with a size of less than 1 μm, stabilised with surfactants, and made using suitable technology. Drug NCs are nanoparticles comprised entirely of drugs without any matrix ingredients.

Precipitation or breakdown processes can produce drug NCs in a liquid dispersion media. The suspension, which comprises drug NCs in a liquid stabilised by surfactants or polymers, is the end result of this method (so called nanosuspension). Drug NCs can be manufactured using a variety of methods. In general, top-down and bottom-up technologies can be distinguished. Bottom-up technology starts with dissolved molecules and precipitates them by mixing a solvent with a non-solvent.

Disintegration (mechanical) procedures, which include various types of wet milling, are top-down technologies. Nuclei creation and crystal development are two phases involved in bottom-up precipitation. While making an appropriate suspension with the least amount of PS, a high nucleation rate is required, while a low growth rate is required [5]. However, in the precipitation method, there will be a chance of crystal growth and long-term stability problems. To summarise, bottom-up approaches are not extensively employed in the manufacture of drug NCs. A mechanical (top-down) process solves such a problem and maintains during the shelf life of the product. Nowadays, top-down technologies (mechanical processes) are more frequently used [6].

In top-down technology, drug nanosuspension is formulated by high shear pearl/ball milling, (developed by G. Liversidge and co-workers) and high-pressure homogenization with different homogenization principles/homogenizer types, including microfludisation and piston-gap homogenizers. Dissocubes, nanopure, and nano-edge techniques were widely used to prepare the drug nanosuspension by piston-gap homogenization principles [7]. Nano-edge: This approach is similar to homogenization or precipitation, and is combined with those two procedures to improve stability and bioavailability. The suspension created by this procedure homogenises to a lower PS and inhibits crystal formation. The nano-edge technology also includes an evaporation technique for superior nanosuspension synthesis, resulting in a solvent-free modified starting material.

The current work used emulsion-diffusion followed by high-pressure homogenization (HPH) with stabilisers to create NCs of CRL in decreased PS (modified nano-edge method). In this approach, the drug must be soluble in at least one solvent, which is combined with a miscible anti-solvent (aqueous) system with surfactants. The rapid addition of drug solution to aqueous solution causes the drug to become supersaturated in the combined solution, resulting in ultrafine drug solids. In concern to this approach, PS and morphology were evaluated, and in vitro dissolution as well, to confirm the increased dissolution rate

of NCs as compared to microcrystals (MCs). The crystalline state of CRL nanoparticles was studied by X-ray diffraction (XRD), fourier transform infrared (FT-IR) spectroscopy, and differential scanning calorimetry (DSC) analysis against CRL-MC and -NCs. Stability studies were also carried out to observe the stability of prepared CRL-NCs.

2. Materials and Methods

2.1. Materials

Dr. Reddy's Laboratories, Hyderabad, India, provided carvedilol (CRL) as a gift sample. Loba Chemicals in Mumbai, India, provided the polyvinylpyrrolidone K-30 (PVP) and sodium dodecyl sulphate (SDS). The rest of the chemicals and reagents were of a high grade in terms of analytical quality.

2.2. Phase Solubility Studies

Higuchi and Connors describe how the PS study will be conducted [8]. In a nutshell, this investigation involved adding a surplus quantity of CRL to 25 mL aqueous solutions of several concentrations (1–15%) to PVP and SDS solutions. The contents of the Eppendorf tubes were put in a water bath at a constant temperature (25 and 37 ± 0.5 °C) for 24 h, trembling every 30 min until equilibrium was recognised. As a consequence, the content was filtered by a 0.45 µm membrane filter (Millipore, Haryana, India), diluted, and the absorbance was measured at 242 nm using a UV spectrophotometer (UV 2310, Techcomp, Delhi, India). The phase solubility curve could be constructed using the computed slope and intercept for the stability complexation constant ($K_{1:1}$; Equation (1)); hence, the CRL intrinsic solubility is proportional to the intercept obtained.

$$K_{(1:1)} = X/((Y\ (1 - X)) \quad (1)$$

where, X and Y denote the slope and intercept, respectively; also, the (ΔH) enthalpy change was estimated by the following equation (Equation (2))

$$\ln K_2/K_1 = \Delta H\ ((T_2 - T_1))/KR\ (T_1)\ (T_2) \quad (2)$$

where K_1, K_2, T_1, and T_2 are the stability constants and difference temperatures of 210 and 310 in Kelvin, respectively [8]. The following equations (Equations (3) and (4)) were used to estimate the Gibbs free energy (ΔG) and change in entropy (ΔS) after complexation/solubilization.

$$\Delta G = -RT\ln K \quad (3)$$

where R = 8.3144 J/mol K and R considered as gas constant

$$\Delta S = \Delta H\ (\Delta H - \Delta G)/(\Delta G) \quad (4)$$

2.3. Docking Study

Molecular docking was used to find physiologically active hits among the proposed ligands, with the lowest binding energy conformation forming a stable complex inside the active region of the β-1-adrenoceptor. CDOCKER, a grid-based molecular docking programme that uses the CHARMm force field, was used in this investigation. The CDOCKER score is given as a negative number (CDOCKER_ENERGY), with a larger number indicating a better binding. The CDOCKER energy was calculated using H-bonds, electrostatic interactions, and van der Waals between the target protein and the ligand. The template protein crystal data [9] was used to identify the simulated protein binding site. To make it simpler for ligands to interact with mutant amino acids, the binding site sphere was put at a radius of 9. The CHARMm force field was used, followed by energy reduction, to identify the local minima (conformation of least energy) of the simulated -1-adrenoceptor with an energy gradient of 0.1 kcal mol^{-1} $Å^{-1}$ using the smart minimizer approach.

2.4. Preparation of CRL Nanocrystals (CRL-NCs)

The CRL-NCs were formulated using an emulsion-diffusion (solvent exchange) technique and HPH with stabilisers. The CRL (80 mg) was dissolved in acetone (2 mL), and this content was added into a beaker containing 50 mL of a 1.6% *w*/*w* aqueous solution of PVP/SDS (1:1). The stabilised CRL solution was sonicated by an ultrasonic cleaner (MrC Dc 1500H, Tokyo, Japan) for 20 min at room temperature [10]. The prepared primary emulsion was subjected to HPH using an ultrasonic high-pressure homogeniser (Biologics, 20 KHZ-3000, VA, USA) with a pulse rate of 80% for 15 min to obtain CRL nanodispersion. Then, the resultant was stirred with a mechanical stirrer (REMI RQ-124 A/D, Mumbai, India) at 500 rpm for 30 min to evaporate acetone by diffusion and to form CRL nanosuspension [11]. Finally, prior to the drying of the nanosuspension, the excess of PVP and SDS were removed by ultracentrifugation (Kemi electronics, Mumbai, India) at 3500 rpm for 30 min, and the supernatant liquid was carefully removed. The residue (sediment) was redispersed two times with double distilled water, and the nanoparticles were dried for 12 h at 60 °C in an oven.

2.5. Percentage Yield and Drug Content

The % Y was calculated to determine the efficacy of the method that was adopted for the preparation of CRL-NCs. The product was collected and weighed to determine the yield by using the following Equation (5).

$$\% \text{ Y} = \text{Mass of NCs recovered/Mass of drug used as formulation} \times 100 \quad (5)$$

The prepared CRL-NCs were dissolved in a suitable quantity of methanol and an appropriate dilution was made with a phosphate buffer pH 6.8 (blank), and drug content was analysed by a UV-visible spectrophotometer at 242 nm.

2.6. Drug Entrapment Efficiency (EE)

The EE of CRL-NCs may be measured using an Eppendorf centrifuge 5430R (Hamburg, Germany) and the ultracentrifugation technique [12]. The supernatant containing free CRL was estimated at 242 nm by a UV-spectrophotometer, and the EE (%) was computed using the method given above. Furthermore, 1 mL NCs was centrifuged (15,000× *g*) at 4 °C for 30 min.

$$\text{EE (\%)} = (\text{amount of CRL incorporated to NC} - \text{Amount of the free CRL})/(\text{Total concentration of PVP/SDS}) \times 100$$

2.7. Particle Size (PS) Analysis

The PS of the CRL-MCs and NCs was measured by a laser diffractometer containing a PS analyser (Nanotrac Inc., Bluewave, Japan). All the samples were diluted with double distilled water to obtain suitable concentration before analysis [13]. Prior to the PS measurement, double distilled water was filtered using a 0.45 µm membrane filter paper (Millipore). Laser diffraction measurement is the volume-based diameter distribution in the size range of 0.01 to 1000 µm, and the PS distribution represents the percentage of particles below the given µm size.

2.8. Dynamic Light Scattering

The hydrodynamic PS, intensity mean of polydispersity index (PDI), and zeta potential (ZP) of CRL, -MC, and the -NCs were estimated using the Zetasizer (Malvern Instruments Ltd., Nano ZS90, Malvern, WR14 1XZ, UK) by dynamic light scattering technology [14].

2.9. Scanning Electron Microscopy (SEM)

The surface structure of the particles was studied using SEM. In the HUS-5GB vacuum evaporator, double sticky tape and gold-coated aluminium stubs were used to mount the samples. The morphology of CRL-MCs and—NCs was studied using a scanning

electron microscope (Hitachi 3000, Tokyo, Japan) with a 10 kV acceleration voltage and the appropriate magnification [14].

2.10. Solid State Profile

2.10.1. Fourier Transform Infrared (FT-IR) Spectroscopy

The FT-IR spectra of CRL samples were analysed using a Perkin Elmer FT-IR series (Model-1600, Waltham, MA USA). Samples were milled (1:100) with IR grade potassium bromide and the corresponding pellets were prepared by a hydraulic compactor (CAP 15T, Bangalore, India) at 5.5 metric tons of pressure [15]. Each pellet was scanned at a resolution of 2 cm at a rate of 4 mm·s^{-1} throughout a wave number range of 4000–400 cm^{-1}.

2.10.2. X-ray Diffraction (XRD) Study

The XRD analysis was employed to detect the effect on the crystallinity of CRL before and after HPH was recorded using diffractometer (Siemens D5000, Munich, Germany). The samples were placed in a sample holder, operating at 30 mA current and 40 kV using Cu Kα radiation as its source [14]. The samples were scanned over an angle range from 0° to 80°, using a step size of 0.02°, and the scan speed was 3° per min.

2.10.3. Differential Scanning Calorimetry (DSC)

The DSC experiments were performed with a differential scanning calorimeter (TAQ 1000, London, UK) with high purity indium metal as the standard [16]. The 3 mg of samples were put in a cremped aluminium sealed pan and heated from 60 to 200 °C at a rate of 5 °C/min while purging with nitrogen (20 mL·min^{-1}). As a control, an empty pan was sealed in the same way as the sample.

2.11. In Vitro Dissolution Study

The rate of dissolution of CRL-MCs and NCs in vitro was measured using a USP dissolution type II (paddle technique) device (Campbell electronic DR-6, Mumbai, India). The equivalent of 10 mg of samples was added to 900 mL of dissolving media as a phosphate buffer pH 6.8 at 37 ± 0.5 °C, with a continuous stirring speed of 50 rpm. To maintain a sink condition, an aliquot of 5 mL was taken from the dissolving apparatus every 15 min for an hr and then replaced with the same volume of a new dissolution media in the flask [17]. With a UV-visible spectrophotometer set to 242 nm and a phosphate buffer pH 6.8 as a blank, the quantity of medication dissolved was calculated.

Dissolution Kinetic Study

Zero- and first-order equations were employed to assist the dissolution kinetic assessments of the NCs formulation, and Higuchi, Hixson Crowell, Korsmeyer Pappas, and release exponent (n) equation models were used to better depict the drug release kinetics [18]. The kinetic release performance of developed CRL-NC formulations and regression coefficient factors (r^2) were determined.

2.12. Stability Studies

After being kept at 4 °C (refrigeration), room temperature, and 40 °C/75 ± 5% RH for a period of six months, the stability study of prepared CRL-NCs was assessed. At every one-month interval, test trials were evaluated for the physical changes, drug content, PS, PDI, ZP, EE (percent), and in vitro drug release [19].

2.13. Analytical Statistics

All of the experiments were done in triplicate, and the outcomes were accessed as mean standard deviation (SD). One-way analysis of variance (ANOVA) was used to analyse the data, with a significance threshold of $p < 0.05$.

3. Results and Discussion

3.1. Preparation of NCs

CRL-NCs were prepared by the emulsion-diffusion method followed by HPH as an effective technology in preparation of CLR in nano size ranges. In this technique, the CRL was dissolved in acetone (class 3 solvent) and then mixed with the aqueous solution containing stabilisers (PVP/SDS) and subjected to ultrasonication. According to the International Conference on Harmonization (ICH), class 3 includes no solvents that are recognised to pose a health hazard at levels commonly used in medicines. Many of the residual solvents in class 3 were never subjected to long-term toxicity or carcinogenicity research. In terms of the solvent, it is advantageous to solubilise the drug in large quantities and have a fast diffusion rate into aqueous solution, whereas the stabilisers must have a high affinity for nanoparticles and efficient adsorption onto the drug particle surface in the water solvent combination [20]. Stabilisers can prevent the growth of nucleating crystals in obtained submicron nanoparticles. The obtained primary emulsion was subjected to HPH, and subsequent evaporation of solvents through diffusion lead to form CRL nanosuspension. This nanosuspension was dried in an oven for the preparation of CRL nanoparticles. Therefore, the combination of PVP/SDS stabilisers, the emulsion-diffusion technique, followed by HPH was performed to obtain optimal CRL-NCs.

3.2. Thermodynamics Outcome

The influence of various carriers on CRL solubility was investigated in this work. Between 210 and 310 Kelvin, a typical linear curve in the concentration order ranges from 2.06×10^{-4} to 6.19×10^{-4} mM. These findings show that changes in the forces of contact between the drug and the carrier, such as hydrophobic forces and van der Waals forces, cause an A_L type of phase solubility profile (CRL solubility cultivates as a function of carrier concentration; Table 1). The PS diagram indicates a slope of 1 in the carriers (PVP and SDS), suggesting 1:1 stoichiometry [21].

Table 1. Thermodynamic parameters of CRL with PVP and SDS s at 25 and 37 °C (mean ± SD, n = 3).

Carriers	T (Kelvin)	Intercept (Mm)	$K_{(1:1)}$ (M^{-1})	ΔG (kJ/mol)	ΔH (kJ/mol)	ΔS (kJ/molK^{-1})
PVP	210	3.66×10^{-4}	0.05029	144.29 ± 6.67	13.9 ± 0.672	0.08891 ± 0.003
	310	6.19×10^{-4}	0.09928	176.17 ± 7.78		
SDS	210	2.06×10^{-4}	0.01989	102.31 ± 5.22	7.31 ± 0.776	0.06254 ± 0.007
	310	2.21×10^{-4}	0.02323	121.17 ± 7.31		

The slope and intrinsic intercept values of the solubility curves were used to compute the stability constant ($K_{1:1}$). The PS graph was drawn by plotting the fraction of CRL dissolved vs. the PVP and SDS concentration (percent w/v; Figure 1). As seen in Table 1 the estimated value of ΔH is positive, suggesting that the binding reaction was endothermic. The ΔS values for PVP and SDS are likewise high (8 and 6 J/mol K, respectively), suggesting that the complex reaction was endothermic. Little decreases in enthalpy (ΔH = −13.9 and 7.31 kJ/mol of PVP and SDS, respectively), and positive changes in entropy (ΔS = 8 and 6 J/molK) seem to be explained by a tighter CRL/carrier cavity fit. A complicated creation that may be seen as the result of enthalpy–entropy compensation [22].

The best interaction constant is found at PVP (Figure 1a; 144 and 176 M^{-1}) and SDS (Figure 1b; 102 and 121 M^{-1}) at 25 and 37 °C, respectively, owing to increased contacts that allow intermolecular interactions between solvent molecules. In the series of 100 to 1000 M^{-1}, both carriers had the best complexation constant. This was assumed to have an effect on the solvent–heteratom interaction [22]. When two non-polar molecules come close together, the disordered water molecules increase in number, resulting in a positive entropy shift and free energy of association. Apart from CRL great solubility in SDS, the hydrophobic interaction (hydrogen bond) is important in CRL solubility. Sodium cholate,

an anionic bile salt, also creates negatively charged droplets, but with a more diverse selectivity than SDS.

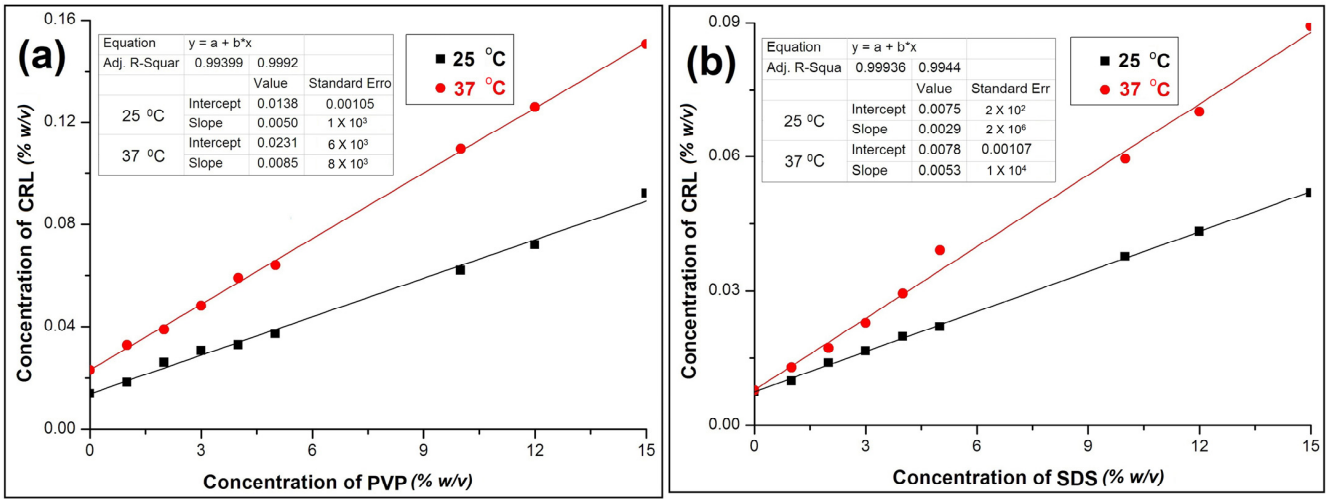

Figure 1. Phase solubility graph of (**a**) CRL-PVP, and (**b**) CRL-SDS.

3.3. Docking Outcome

The compound was docked to the β_1 adrenoreceptor, and the docking tests demonstrated that the CRL has a common binding orientation in the catalytic binding pocket of the active site [23]. As demonstrated in Figure 2a and ligplot, the ketone moiety plays a key part in binding because the carbonyl oxygen atom is engaged in hydrogen bonding interactions with amino acid residues Gln483 and Arg501 at the catalytic region (Figure 2a). In the CRL, a pi–pi mounding contact was also detected between the phenyl ring of Glu479 and Pro500. Furthermore, the phenyl group moiety demonstrated hydrophobic association with Lys478 amino acid residues in the β_1 adrenoreceptor protein, and Pro500 pi interaction with the OCH_3 bond [24]. Van der Waals interactions with CRL are formed by amino acids, such as Trp486, Thr502, Asn482, Asp505, and Leu194 (Figure 2b). The performed molecular docking simulations produced compounds at the β-1 adrenoreceptor catalytic ligand binding site using Gln503 and Gln504 binding modes of carbon five-membered ring. The CRL's docking score was revealed as -23.481 Kcal/mol^{-1}.

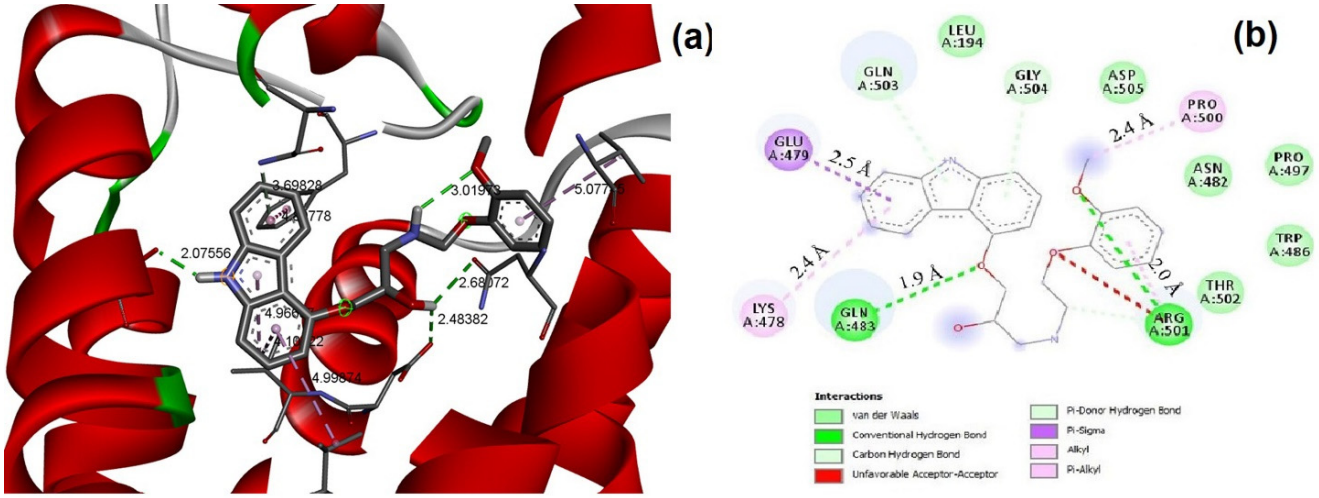

Figure 2. (**a**) The binding mode of β_1 adrenoreceptor active site, and (**b**) Ligplot of β_1 adrenoreceptor active site.

3.4. Percent Yield, Drug Content and % EE

Table 2 shows the percent yield and drug content of CRL-MC and -NCs. Micro and NCs produced over 80% of the total output, with the highest absorption of CRL-NCs measured between 200 and 400 nm, with a peak at 242 nm (data not showed). Due to limited size ranges, the drug content of produced MC and NCs was determined to be 98.90 ± 0.32 and 96.81 ± 0.64%, respectively, which was within the reference (label amount) of 95.5 to 102% of CRL. The percent EE of CRL-MC and -NCs, respectively, was 84.12 ± 0.33 and 83.61 ± 0.80 percent (Table 2). CRL lipophilicity (log P = 3.8) can be attributed to these low percent EE values, allowing it to be efficiently integrated into PVP/SDS dual carriers in the prepared formulations. According to Mohamed et al. (2022), a lipophilic drug might enhance EE by employing a lipid as an encapsulating carrier [25].

Table 2. Various characterization parameters CRL-MC and –NCs (mean ± SD, *n* = 3).

Batches	% Yield	Drug Content * (%)	% EE *	PS (µm) *	PS (nm) *	PDI *	Zeta Potential (mV) *
CLR-MCs	79.6 ± 2.58	98.90 ± 4.32	84.12 ± 2.33	106.60 ± 3.27	1102.13 ± 8.22	0.206 ± 0.017	−25.6 ± 3.19
CLR-NCs	78.7 ± 3.41	96.81 ± 3.64	83.61 ± 1.80	0.058 ± 0.074	58.29 ± 0.034	0.181 ± 0.012	−27.2 ± 2.29

* Each value represents mean, *n* = 3 ± SD.

3.5. PS Analysis

The CRL-MCs were distributed between 1 and 1000 µm as illustrated in Figure 3a, while prepared NCs by emulsion-diffusion followed by HPH showed in narrow PS distribution at a range of 0.02–1 µm (20–1000 nm). The average particle diameter of CRL-MCs was found to 106.62 ± 3.27 µm, whereas the prepared CRL-NCs were 0.058 µm (58 nm), shown in Figure 3b, with the standard deviation of 0.0104 µm. Figure 3c illustrate the comparison of PS distribution, showing that the prepared CRL nanoparticles were in a narrow range with nanometric size.

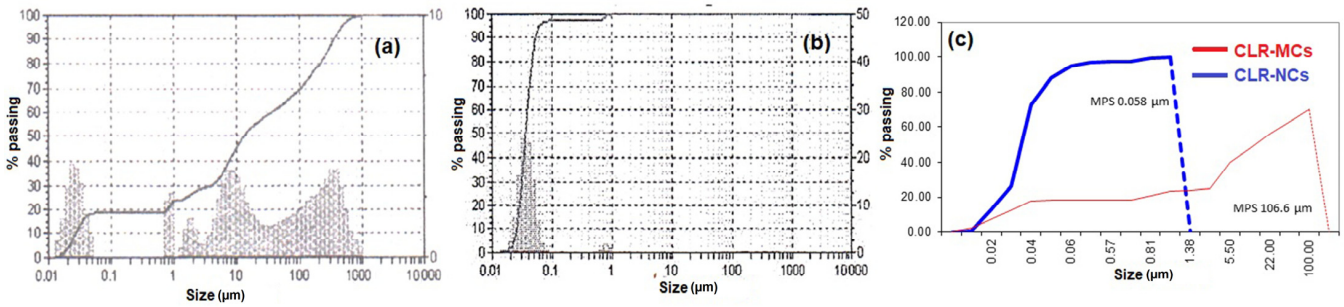

Figure 3. PS of (**a**) CRL-MCs, (**b**) CRL-NCs (gray area indicates the PS distribution), and (**c**) comparative graphical representation of both CRL-MC and -NCs.

3.6. PS, PDI and ZP

Table 2 and Figure 4a show that the average PS of the CRL-NCs ranged from 58.29 to ±0.034 nm. CRL-NCs had PDI values below 0.4, implying that the solution was homogenous and monodisperse [21]. The inclusion of the negative charge inducer PVP resulted in ZP value ranges that were found as −27.2 (Figure 4b). The considerable value of charge, according to Mohammed et al. (2021), implies strong stability against NC's aggregation and fusion [26].

This size of the CRL-NC particle had a large interfacial surface area, which helps with drug absorption and lymphatic transit [18]. PDI value less than 0.5 are considered usual for nanocrystals. Because the surfactant monolayer for nanostructures has a very low interfacial tension, there is less of a consequence (more chance) for having a non-spherical shape, compared to normal emulsions, which typically have spherical structures due to high interfacial tensions favouring globule interfacial area reduction (the sphere has the lowest interfacial area for a given volume).

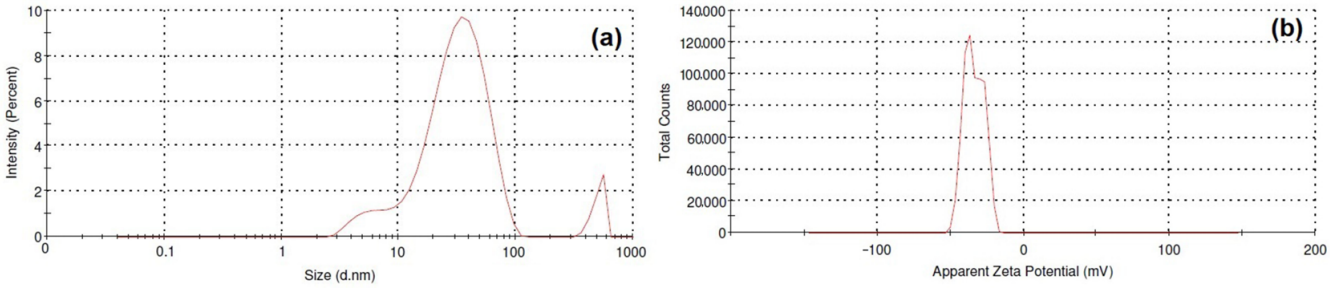

Figure 4. (**a**) PS and PDI, (**b**) ZP of CRL−NCs.

3.7. SEM

The SEM photographs for CRL-MC and NCs are shown in Figure 5, which shows the distinct difference in the morphology of samples. In the SEM of the CRL-MCs, the boundary and core of well-identified spherical formations can be observed. The prepared CRL-NCs were nearly spherical in shape, the surface of a particle was smooth and the PS in nanometric range (Figure 5b), whereas CRL-MCs were predominantly needle shape crystals with a lighter exposed core, surrounded by a denser boundary that perfectly ringed the centre (Figure 5a). When a thin polymer layer is hydrated, it forms an encircled crystal network, allowing the system to change shape from globular to spherical and attain thermodynamic stability by reducing total free energy [27]. Even after applying diverse mechanical stressors, such as sonication and HPH, the spherical structure's stability was proven.

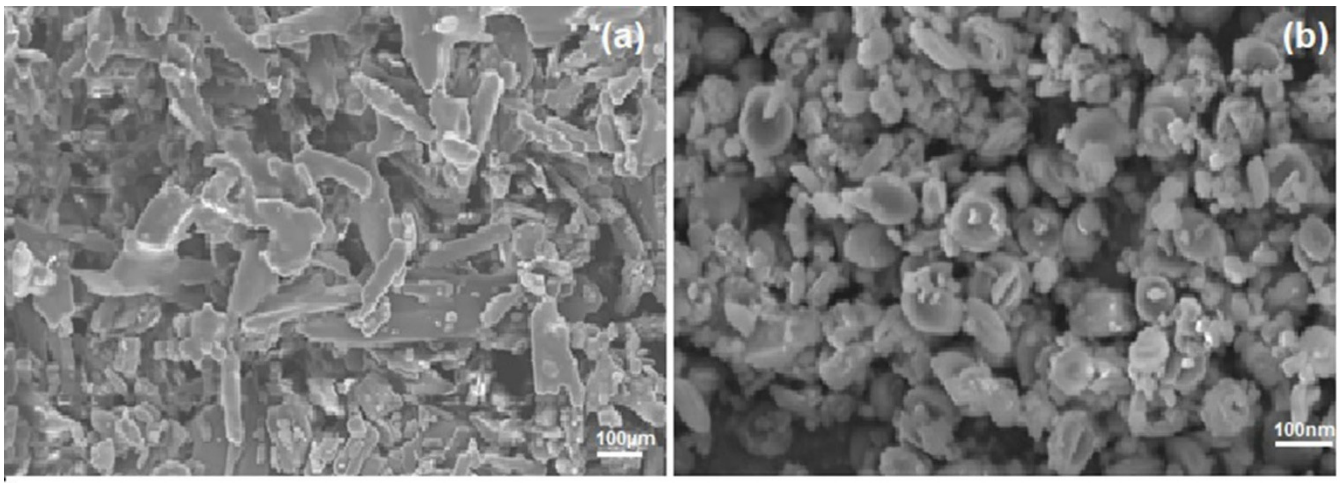

Figure 5. SEM photograph of (**a**) CRL-MC, and (**b**) CRL-NCs.

3.8. FT-IR

The characteristic peak of CRL-MCs was shown in Figure 6a, and the characteristic peaks at 3344.16 (NH stretching), 2922.90 (CH stretching), 1502.43 (C=C stretching), 1251.63 (C=N bending), and 1099.62 cm^{-1} (C=O bending). In the prepared CRL-NCs, shown in Figure 6a, peaks were obtained at 3398.73, 2926.24, 1505.77, 1254.38, and 1100.84 cm^{-1}. The reduced recurrence in the C=O stretching peak vibration corresponding to the CDL was evidence of the strong complexation of the drug with the carrier molecules. It demonstrates that none of the excipients employed in the emulsion-diffusion followed by the HPH approach had any chemical interaction with CRL-NCs [28].

3.9. XRD

When the formulation was formed as nanoparticles, the XRD was utilised to analyse the molecular structure and crystalline nature of the drug. The amount of this feature was

determined by the CRL chemical composition and physical hardness, as well as powder density. The characteristic diffraction peaks were obtained for CRL-MC and -NCs. As shown in Figure 6b, of CRL-MC's intensity from 0 to 40°, distinctive peaks at 14.9, 17.2, 18.2, 23.6, and 26°, are comparable with the XRD pattern of crystalline CRL reported in the previous study [29]. The prepared CRL-NC diffractogram peaks around 2θ were at a range of 14.90, 17.12, 17.26, 21.98, and 26.36°, which are super imposable and reveal the characteristic peak of CRL, thus indicating the absence of chemical instability in the solid state (Figure 6b). As can be seen, the CRL-NCs were retained in a crystalline state using emulsion-diffusion followed by an HPH and drying process. The reduction in crystallinity and improved wettability of the CRL-NCs after homogenization can also be well correlated with in vitro dissolution, which was higher as compared to the CRL-MCs.

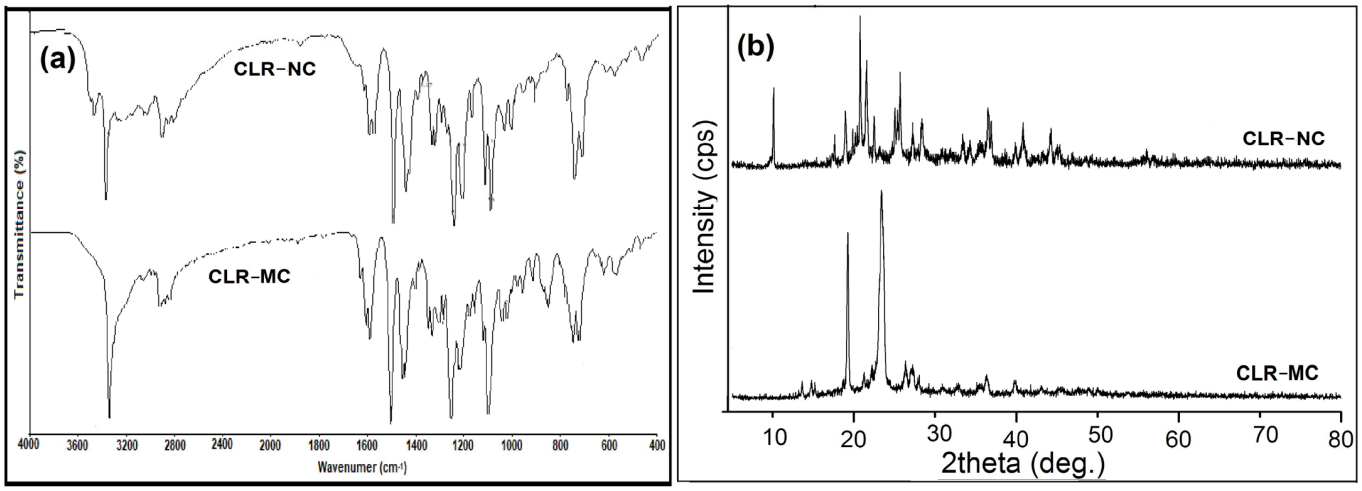

Figure 6. (**a**) FT-IR spectra and (**b**) XRD pattern of CRL-MC and -NCs.

3.10. DSC

The DSC investigations were carried out to learn more about the drug's physical condition and how it may affect the in vitro and in vivo testing of the drug formulation. DSC thermograms of CRL-MCs and NCs were illustrated in Figure 7. The CRL-MCs observed a sharp characteristic endothermic peak at 112.20 °C, showing crystalline nature. The onset and endset of phase transitions in CRL-MCs were observed at 104.06 and 139.05 °C, respectively (Figure 7a). After HPH being as an NC, its melting point decreased to 108.02 °C, with a fusion enthalpy of 104.4 $J \cdot g^{-1}$. The DSC thermogram of CRL NCs showed a characteristic endothermic peak corresponding to those of the MCs with significant change, and there is no appearance or disappearance of additional peaks (Figure 7b). This indicates that crystalline nature remains, with reduced crystallinity.

The DSC thermogram CRL-NCs indicates that its melting point was decreased to 108.02 °C due to reduced crystallinity. In addition, the obtained SEM and XRD results show the CRL remain in crystalline (NCs) nature even after homogenization. Similar finding is also reported for celecoxib nanoparticles [30]. Therefore, the significant change in the melting characteristic of CRL-NCs indicates no polymorphic changes using emulsion-diffusion followed by HPH.

3.11. In Vitro Dissolution Study

The in vitro release profile of CRL-MCs and -NCs are shown in Figure 8. The comparative in vitro dissolution release of CRL-NCs and -MCs was 46.24 ± 1.51 and 14.81 ± 1.25%, respectively, in the first 15 min. CRL-NC's dissolution rate was markedly enhanced ($p < 0.05$) as compared to the MCs. The CRL-NCs gave the highest percent (96%) of cumulative drug release, more than MCs after 1 h. It was found that cumulative percent drug release for the CRL-NCs was a three-fold increase from the original form, due to the

reduction of its PS. The CRL-NCs have the potential to release the CLR in a controlled manner throughout 60 min, as demonstrated in this study. As a result of the improved solubility of CRL, it may be possible to provide a continuous/uninterrupted drug release over a longer period of time [17]. The sluggish release of CRL in the instance of a free medication was due to its low water solubility due to the CRL being classified as BCS II [14].

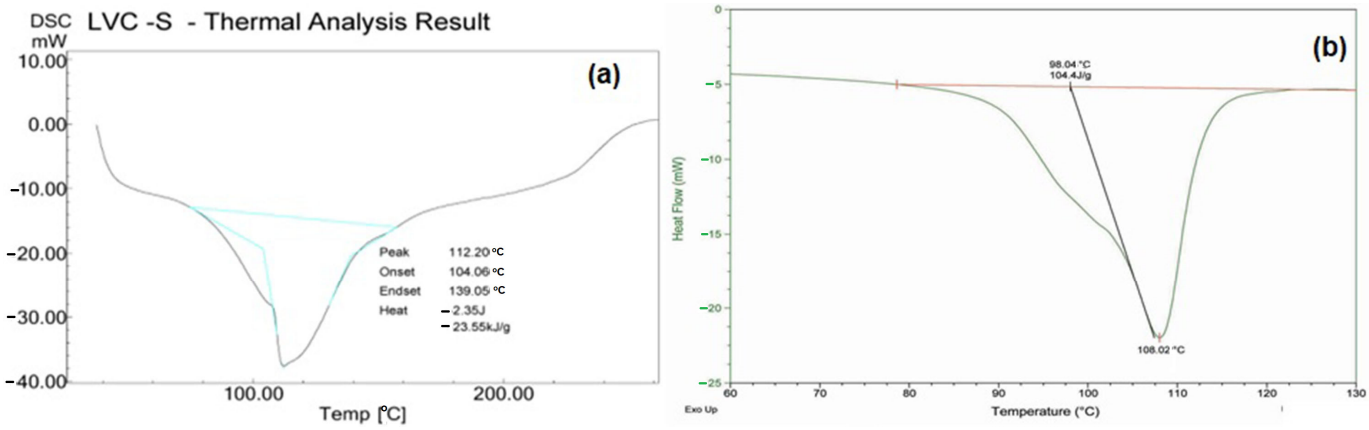

Figure 7. DSC thermogram of (**a**) CRL-MC and (**b**) CRL-NC; Blue line—total area of the peak, Red line—onset to end set of temperature, and Black line—midpoint (onset) of temperature.

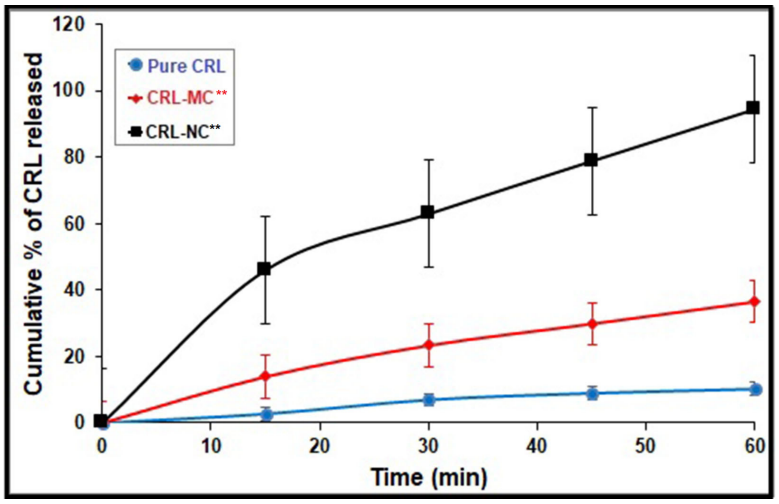

Figure 8. In vitro dissolution of pure CRL, CRL-MC, and -NCs (mean ± SD, n = 3); the significant differences related to control (pure CRL) are represented by ** $p < 0.05$ evaluated by the ANOVA test.

The data from Table 3 clearly indicates the Higuchi equation with the highest linearity (r^2 = 0.9897 and 0.9759), best described in vitro drug release for both CRL-MC and -NCs. The Korsemayer-eppas equation had a slope of more than 0.5 but less than 0.85, suggesting non-Fickian diffusion, with the drug released by diffusion and erosion [31].

3.12. Stability Studies

The CRL-NCs maintained ($p > 0.05$) for further characterisation and stability testing. According to the data in Table 4, the CRL-NCs remained stable for six months with 60% RH at 45 ± 0.5 °C. Only a minor growth in PS, ZP, and PDI (68.39 ± 3.88 nm, −19.2 ± 4.66 mV and 0.334 ± 0.091, respectively) was noticed after storage. On the other hand, there was very little impact on drug content, % EE, ZP, and cumulative in vitro CLR release after storage, such as 93.65 ± 2.45, 76.40 ± 4.74, and 85.71 ± 5.53 %, respectively. This outcome suggests that, when stored at 4 °C, CRL-NCs have a good physical stability [32].

Table 3. In vitro release kinetics of pure CRL, CRL-MC, and -NCs (mean ± SD, *n* = 3).

	Coefficient of Correlation (r^2)					
Preparations	**Zero Order**	**First Order**	**Hixon Crowell**	**Higuchi**	**Korsmeyer-Peppas**	**Release Exponent (*n*)**
Pure CRL	0.9834 ± 0.62	0.7356 ± 0.78	0.8891 ± 0.33	0.9678 ± 0.46	0.8891 ± 0.21	0.441 ± 0.47
CRL-MCs	0.9769 ± 0.32 **	0.7589 ± 0.41 *	0.8849 ± 0.87 *	0.9897 ± 0.54 **	0.8793 ± 0.58 *	0.417 ± 0.36 **
CRL-NCs	0.9866 ± 0.98 **	0.7892 ± 0.54	0.9471 ± 0.62	0.9759 ± 0.77 **	0.9359 ± 0.22	0.466 ± 0.35 **

* Each value expressed as mean, (*n* = 3; ±SD); the significant differences related to control (Pure CRL) are represented by ** $p < 0.05$ evaluated by the ANOVA test.

Table 4. Various stability parameters of CRL-NCs.

Evaluations	**0 Month**	**1 Month**	**3 Month**	**6 Month**
Drug content *	98.90 ± 0.32	97.94 ± 1.43	96.11 ± 1.57	93.65 ± 2.45 *
PS * (nm)	58.29 ± 0.034	60.78 ± 0.22	62.78 ± 1.19	68.39 ± 3.88
PDI *	0.181 ± 0.012	0.235 ± 0.045	0.241 ± 0.02	0.334 ± 0.091
ZP * (mV)	−27.2 ± 2.29	−24.1 ± 3.12	−22.4 ± 4.41	−19.2 ± 4.66
EE (%) *	83.61 ± 1.80	80.12 ± 1.22	79.35 ± 2.81	76.40 ± 4.74 **
In vitro release (after 60 min) *	94.56 ± 3.27	92.22 ± 4.16	89.33 ± 5.28	85.71 ± 5.53 **

* Each value expressed as mean, (*n* = 3; ±SD); the significant differences associated to control (pure CRL) are represented by ** $p < 0.05$ evaluated by the ANOVA test.

4. Conclusions

The CRL-MC and -NCs of carvedilol, a poorly water-soluble drug, were prepared by emulsion-diffusion followed by the HPH approach. The stabilisers PVP and SDS were utilised to prepare stable and high-quality NCs. The stabilisers used had no effect on the chemical structure of the drug and various evaluation studies concluded that the prepared CRL-NCs was promising novel delivery of CRL in pharmaceuticals aspects. The added benefit of this CRL-NC formulation is that it may be used for a variety of delivery methods, including oral and parenteral. As a result, the formation of NCs via emulsion diffusion followed by HPH with stabilisers might be used to increase the solubility, stability, and bioavailability of poorly soluble or lipohillic drugs. More clinical trials to test the efficacy of CRL-NCs in hypertensive patients are now underway.

Author Contributions: Conceptualization, investigation, methodology, writing—original draft finished by A.K.J., J.M.M.M. and S.K. Software, funding acquisition, resources and visualization done by A.A. (Ali Alqahtani), A.A.F., F.M., T.A. and A.A. (Ali Alamri). Data curation, formal analysis, statistical analysis and writing—review, editing, and validation carried out by F.M., M.E.-S. and S.R. All authors have read and agreed to the published version of the manuscript.

Funding: The authors are grateful to the Deanship of Scientific Research at King Khalid University for funding this study through the Large Research Group Project, under grant number RGP2/3/43.

Institutional Review Board Statement: Not applicable.

Informed Consent Statement: Not applicable.

Data Availability Statement: Data sharing not applicable.

Acknowledgments: The authors are grateful to the Faculty of Pharmaceutical Sciences, UCSI University, Cheras 56000, Kuala Lumpur, Malaysia for providing necessary facilities to develop this research work.

Conflicts of Interest: The authors declare no conflict of interest.

References

1. Ali, M.A.; Kataoka, N.; Ranneh, A.H.; Iwao, Y.; Noguchi, S.; Oka, T.; Itai, S. Enhancing the Solubility and Oral Bioavailability of Poorly Water-Soluble Drugs Using Monoolein Cubosomes. *Chem. Pharm. Bull.* **2017**, *65*, 42–48. [CrossRef] [PubMed]
2. Zhang, Q.W.; Lin, L.G.; Ye, W.C. Techniques for extraction and isolation of natural products: A comprehensive review. *Chin. Med.* **2018**, *13*, 20. [CrossRef] [PubMed]
3. Sun, J.; Wang, F.; Sui, Y.; She, Z.; Zhai, W.; Wang, C.; Deng, Y. Effect of particle size on solubility, dissolution rate, and oral bioavailability: Evaluation using coenzyme Q_{10} as naked nanocrystals. *Int. J. Nanomed.* **2012**, *7*, 5733–5744. [PubMed]
4. Jacob, S.; Nair, A.B.; Shah, J. Emerging role of nanosuspensions in drug delivery systems. *Biomater. Res.* **2020**, *24*, 3. [CrossRef]
5. Ashok, K.J.; Ramkanth, S.; Lakshmana, P.S.; Gopal, V. Enhancement of Saturation Solubility and In Vitro Dissolution of Carvedilol Nanoparticles by High Pressure Homogenization Technique. *Int. J. Curr. Pharm. Rev. Res.* **2015**, *6*, 269–273.
6. Tofail, S.A.M.; Koumoulos, E.P.; Bandyopadhyay, A.; Bose, S.; O'Donoghue, L.; Charitidis, C. Additive manufacturing: Scientific and technological challenges, market uptake and opportunities. *Mater. Today* **2018**, *21*, 22–37. [CrossRef]
7. Li, J.; Wang, Z.; Zhang, H.; Gao, J.; Zheng, A. Progress in the development of stabilization strategies for nanocrystal preparations. *Drug Deliv.* **2021**, *28*, 19–36. [CrossRef]
8. Higuchi, T.; Connors, K.A. Phase solubility techniques. *Adv. Anal. Chem. Instrum.* **1965**, *4*, 117–212.
9. Balasubramaniyan, S.; Irfan, N.; Umamaheswari, A.; Puratchikody, A. Design and virtual screening of novel fluoroquinolone analogs as effective mutant DNA GyrA inhibitors against urinary tract infection causing fluoroquinolone resistant *Escherichia coli*. *RSC Adv.* **2018**, *8*, 23629–23647. [CrossRef]
10. Mohamed, J.M.M.; Mahajan, N.; El-Sherbiny, M.; Khan, S.; Al-Serwi, R.H.; Attia, M.A.; Altriny, Q.A.; Arbab, A.H. Ameliorated Stomach Specific Floating Microspheres for Emerging Health Pathologies Using Polymeric Konjac Glucomannan-Based Domperidone. *BioMed Res. Int.* **2022**, *2022*, 1–12. [CrossRef]
11. Lefroy, K.S.; Murray, B.S.; Ries, M.E. Advances in the use of microgels as emulsion stabilisers and as a strategy for cellulose functionalisation. *Cellulose* **2021**, *28*, 647–670. [CrossRef]
12. Mohamed, J.M.; Alqahtani, A.; Ahmad, F.; Krishnaraju, V.; Kalpana, K. Pectin co-functionalized dual layered solid lipid nanoparticle made by soluble curcumin for the targeted potential treatment of colorectal cancer. *Carbohydr. Polym.* **2020**, *252*, 117180. [CrossRef] [PubMed]
13. Teeranachaideekul, V.; Junyaprasert, V.B.; Souto, E.B.; Müller, R.H. Development of ascorbyl palmitate NCs applying the nanosuspension technology. *Int. J. Pharm.* **2008**, *354*, 227–234. [CrossRef] [PubMed]
14. Mohamed, J.M.; Alqahtani, A.; Ahmad, F.; Krishnaraju, V.; Kalpana, K. Stoichiometrically governed curcumin solid dispersion and its cytotoxic evaluation on colorectal adenocarcinoma cells. *Drug Des. Deliv. Ther.* **2020**, *14*, 4639–4658. [CrossRef]
15. Potluri, R.H.K.; Bandari, S.; Jukanti, R.; Veerareddy, P.R. Solubility enhancement and physicochemical characterization of carvedilol solid dispersion with Gelucire 50/13. *Arch. Pharm. Res.* **2011**, *34*, 51–57. [CrossRef]
16. Bathool, A.; Vishakante, G.D.; Khan, M.S.; Shivakumar, H.G. Development and characterization of atorvastatin calcium loaded chitosan nanoparticles for sustain drug delivery. *Adv. Mater. Lett.* **2012**, *3*, 466–470. [CrossRef]
17. Moideen, J.M.M.; Alqahtani, A.; Venkatesan, K.; Ahmad, F.; Krisharaju, K.; Gayasuddin, M.; Shaik, R.A. Application of the Box-Behnken design for the production of soluble curcumin: Skimmed milk powder inclusion complex for improving the treatment of colorectal cancer. *Food Sci. Nutr.* **2020**, *8*, 6643–6659. [CrossRef]
18. Muthu, M.J.; Kavitha, K.; Chitra, K.S.; Nandhineeswari, S. Soluble curcumin prepared by solid dispersion using four different carriers: Phase solubility, molecular modelling and physicochemical characterization. *Trop. J. Pharm. Res.* **2019**, *18*, 1581–1588.
19. Mohamed, J.M.M.; Alqahtani, A.; Kumar, T.V.A.; Fatease, A.A.; Alqahtani, T.; Krishnaraju, V.; Ahmad, F.; Menaa, F.; Alamri, A.; Muthumani, R.; et al. Superfast synthesis of stabilized silver nanoparticles using aqueous allium sativum (garlic) extract and isoniazid hydrazide conjugates: Molecular docking and in-vitro characterizations. *Molecules* **2022**, *27*, 110. [CrossRef]
20. Bergström, C.A.S.; Strafford, M.; Lazorova, L.; Avdeef, A.; Luthman, A.K.; Artursson, P. Absorption classification of oral drugs based on molecular surface properties. *Med. Chem.* **2003**, *46*, 558–570. [CrossRef]
21. Mohamed, J.M.; Ahmad, F.; Kishore, N.; Al-Subaie, A.M. Soluble 1: 1 stoichiometry curcumin binary complex for potential apoptosis in human colorectal adenocarcinoma cells (SW480 and Caco-2 cells). *Res. J. Pharm. Technol.* **2021**, *14*, 129–135.
22. Mohamed, J.M.M.; Ahmad, F.; Alqahtani, A.; Alqahtani, T.; Krishnaraju, V.; Anusuya, M. Studies on preparation and evaluation of soluble 1:1 stoichiometric curcumin complex for colorectal cancer treatment. *Trends Sci.* **2021**, *18*, 1403. [CrossRef]
23. Goshain, O.; Ahmed, B. Antihypertensive activity, toxicity and molecular docking study of newly synthesized xanthan derivatives (xanthonoxypropanolamine). *PLoS ONE* **2019**, *14*, e0220920. [CrossRef] [PubMed]
24. Avula, P.R.; Asdaq, S.M.; Asad, M. Effect of aged garlic extract and s-allyl cysteine and their interaction with atenolol during isoproterenol induced myocardial toxicity in rats. *Indian J. Pharmacol.* **2014**, *46*, 94–99.
25. Mohamed, J.M.M.; Alqahtani, A.; Khan, B.A.; Fatease, A.; Alqahtani, T.; Venkatesan, K.; Ahmad, F.; Alzghoul, B.I.; Alamri, A. Preparation of soluble complex of curcumin for the potential antagonistic effects on human colorectal adenocarcinoma cells. *Pharmaceuticals* **2021**, *4*, 939. [CrossRef]
26. Mohamed, J.M.M.; Alqahtani, A.; Fatease, A.; Alqahtani, T.; Khan, B.A.; Asmitha, B.; Vijaya, R. Human hair keratin composite scaffold: Characterisation and biocompatibility study on nih 3t3 fibroblast cells. *Pharmaceuticals* **2021**, *14*, 781. [CrossRef]
27. Mohamed, J.M.; Bharathidasan, P.; Raffick, M.M. Preformulation and development of curcumin magnetic nanosuspension using magnetite (Fe_3O_4) and methyl cellulose. *Int. J. Pharma Bio Sci.* **2012**, *3*, 419–432.

28. Senthilvel, C.K.; Karupiayan, K.; Moideen, M.M.J. Development of capsules filled with phenytoin and berberine loaded nanoparticles- A new approach to improve consultant therapy. *Indian J. Pharm. Educ. Res.* **2019**, *53*, 468–479. [CrossRef]
29. Tozuka, Y.; Ito, A.; Seki, H.; Oguchi, T.; Yamamoto, K. Characterization and quantitation of clarithromycin polymorphs by powder X-ray diffractometry and solid-state NMR spectroscopy. *Chem. Pharm. Bull.* **2002**, *50*, 1128–1130. [CrossRef]
30. Dolenc, A.; Kristl, J.; Baumgartner, S.; Planinšek, O. Advantages of celecoxib nanosuspension formulation and transformation into tablets. *Int. J. Pharm.* **2009**, *376*, 204–212. [CrossRef]
31. Kumar, C.S.; Raja, M.D.; Sundar, D.S.; Antoniraj, M.G.; Ruckmani, K. Hyaluronic acid co-functionalized gold nanoparticle complex for the targeted delivery of metformin in the treatment of liver cancer (HepG2 cells). *Carbohydr. Polym.* **2015**, *128*, 63–74. [CrossRef] [PubMed]
32. Phan, H.T.; Haes, A.J. What Does Nanoparticle Stability Mean? *J. Phys. Chem. C Nanomater. Interfaces* **2019**, *123*, 16495–16507. [CrossRef] [PubMed]